Probing Effective Loop Quantum Gravity on Weak Gravitational Lensing, Hawking Radiation and Bounding Greybody Factor by Black Holes

Wajiha Javed,[1,*] Mehak Atique,[1,†] and Ali Övgün[2,‡]

[1]*Department of Mathematics, Division of Science and Technology, University of Education, Lahore-54590, Pakistan*
[2]*Physics Department, Eastern Mediterranean University, Famagusta, 99628 North Cyprus via Mersin 10, Turkey.*

(Dated: June 14, 2022)

In this work, we examine the deflection angle of black hole in effective loop quantum gravity in non-plasma medium via the geometrical technique of Gibbons and Werner in weak field limits. For this, we attain the optical metric and calculate the Gaussian optical curvature and then we apply the Gauss-Bonnet theorem. We also study the influence of the plasma and dark matter mediums on the deflection angle. Further, we obtain the deflection angle by using Keeton and Petters method. We also calculate the Hawking temperature via Gauss-Bonnet theorem. In addition, we determine the fermionic greybody bounds. Moreover, we discuss the graphical behaviour of the bending angle and bounds on the greybody factor. We also examine that the results obtained for the black hole in effective loop quantum gravity are reduces to the Schwarzschild black hole solutions when dimensionless non-negative parameter $A_\lambda = 0$.

PACS numbers: 95.30.Sf, 98.62.Sb, 97.60.Lf
Keywords: General Relativity; Black hole; Deflection angle; Hawking radiation; Plasma medium; Gauss-Bonnet theorem; Dark matter; Greybody factor

I. INTRODUCTION

After hundred of years, the progress in physics attained by Einstein's theory of relativity corroborated its importance, when first image of a supermassive black hole (BH) which is in the center of the M87 galaxy, 55 million light years from earth was taken by Event Horizon Telescope on April 10, 2019 [1]. This has maked a new history in theoretical cosmology and attracted the interest of researchers in BHs [2]-[7]. A BH is a massive area with gravitational field so strong that nothing even the light cannot get out from it. Black holes have three main parts: singularity, outer event horizon and the inner event horizon. There are four different kinds of BHs that are miniature BHs, stellar BHs, intermediate BHs and supermassive BHs. Miniature BHs are also called micro BHs. These types of BHs have event horizons as tiny as atomic particles. Stellar BHs are the BHs having masses ranging from five to several tens of solar masses while the intermediate BHs have the masses ranging from 10^2 to 10^5 solar masses. Supermassive BHs are the BHs which are millions to billions times more massive than the sun. Black holes are one of the objects that bring about the rare event of gravitational lensing (GL).

Light does not always travel in a straight line, when the light beam passes from the area of a huge object it is bended due to the connection among light and gravitational field of the the objects. So each object can behave like a lens and results in the phenomenon called GL. Depending on how much light bends, the GL is partitioned into weak, strong and micro GL [8]-[13]. Gravitational lensing is said to be strong GL when the lens is so strong to produce the multiple images, Einstein rings or even arcs. This type of lensing requires lens, source and spectator aligned. In weak lensing, in most cases the lens is not strong enough to produce multiple images. Micro GL is different from weak and strong GL. In this type of lensing, the lens is small as compared to weak and strong GL. Gravitational lensing is a helpful framework to understand the cosmic systems, dark matter, dark energy and the universe [14]. Numerous work on GL for BHs, wormholes and other objects have been composed [15]-[19].

Gibbons and Werner showed an alternate method for getting the deflection angle from non-spining asymptotically flat space-times via Gauss-Bonnet theorem (GBT) and optical geometry [20]. Werner stretched out this technique to the stationary space-times using Kerr-Randers optical geometry[21]. The Gibbons and Werner technique has been applied by various researchers on BHs and wormholes [22]-[55]. The bending angle for asymptotically flat BH can be defined as [20]:

$$\breve{\delta} = -\int\int_{F_\infty} \mathcal{K} dS,$$

*Electronic address: wajiha.javed@ue.edu.pk
†Electronic address: mehakatique1997@gmail.com
‡Electronic address: ali.ovgun@emu.edu.tr

Preprints (www.preprints.org) | NOT PEER-REVIEWED | Posted: 15 June 2022 doi:10.20944/preprints202206.0211.v1

where, $\breve{\delta}$ is the deflection angle, $\mathcal{K}$ stands for Gaussian optical curvature, dS stands for surface component and F_∞ represents the infinite domain of the space. The main point is to noted that the above equation for deflection angle simply satisfy the asymptotically flat metric, whereas for non-asymptotically flat metric just a limited distance rectifications can be studied.

In the background of quantum field theory, Hawking came up with the concept that something get away from the BH, these are radiation [56]. This turned into the one of the vital finding of Hawking and these radiation are named as Hawking radiation. His work [56, 57] combined two distinct theories like quantum mechanics and general relativity. Creation and annihilation of particles are feasible in the framework of quantum field theory. If pair production takes place near a horizon of a BH, one can observed that one of the particles from pair production comes out of the BH from which Hawking radiation results while the remaining falling back to the BH. According to the general relativity, BH bends spacetime about it, which acts as the gravitational potential, inside which particles move. Some of the radiation are transmitted out of the BH and escape to infinity and rest are reflected back in the BH. Therefore, the Hawking radiation observed by an observer which passing from the gravitational potential is different from the one which has not been passed from the gravitational potential. The difference can be investigated by the greybody factor.

Different techniques have been proposed to acquire the Hawking radiation [58]-[62]. Hawking temperature obtained via utilizing the Euclidean path integral for the gravitational field by Hawking and Gibbons [63]. Robson, Villari, and Biancalana [64, 65] have shown that topologically Hawking temperature of a BH can also be attained. By topological technique depends on the invariants of the topology which are GBT and Euler characteristic. Using topological technique one can obtain the Hawking temperature for Euclidean geometry of the 2-dimensional spacetime without losing the facts of 4-dimensional spacetime. Ovgun and Sakalli [66] obtained the Hawking temperature for various BHs by applying the topological technique.

Greybody factor has been obtained by using various methods. Some utilized the matching technique to acquire the greybody factor [67]-[69], whereas some utilized WKB approximation [70]-[71]. A new technique has also been developed to compute the greybody factor without the approximations. This new technique acquires the computation of the bound on the greybody factor. Using this method many researchers have calculated the bounds on the greybody factor for the various BHs [72]-[84].

Spacetime singularity inside a BH is one of the most vital issue. Generally, it is considered that the singularity can be avoided by some quantum effects. Several attempts have been made to recognize the spacetime singularity but a well-advanced quantum theory of gravity is still impossible to achieve. Phase space quantization is one of the most fruitful endeavors that refers to the polymerization procedures created in loop quantum gravity, which has been utilized to fix the big-bang singularity [85]-[87]. A small parameter called the polymer scale is presented in this quantization procedure. The quantum impacts can no longer be ignored when come closer to this scale. At high energy scales to understand the nature of the spacetime, BH as an major candidate of the strong gravitational rule plays a vital role. It is natural to explain the BH spacetimes by means of considering the quantum corrections, together with the polymerization schemes. From many previous years, plenty of effective polymerized BHs had been built [88]-[93], most of which concentrated on the spherically symmetric spacetimes.

A Swiss astronomer, named Zwicky was one of the first to discover dark matter [94]. Dark matter can't be seen directly and initially, the dark matter was called missing matter. Dark matter is composed of particles that do not reflect, absorb or emit light or any other electromagnetic radiaion. The total mass energy of the universe consisting of 27% of dark matter [95]. Dark matter has weak non-gravitational interactions and we only investigate it by gravitational interactions and it is non-baryonic, non-relativistic. The different types of dark matter candidates are super-interacting massive particles, weakly interacting massive particles, sterile neutrinos and axions. The refractive index for the dark matter medium which is defined as [96]:

$$n(\omega) = 1 + \beta A_0 + A_2\omega^2. \tag{1}$$

Here, $\beta = \frac{\rho_0}{4m^2\omega^2}$, ρ_0 indicates the mass density of the dispersed dark substance particles, $A_0 = -2\epsilon^2 e^2$ and $A_{2j} \geq 0$. The $\mathcal{O}(\omega^2)$ and higher terms are linked to the polarizability of the dark substance candidate. Remark that ω^2 is for neutral dark substance candidate and ω^{-2} is because of the charged dark substance candidate. Furthermore, when parity and charge-parity asymmetries exist there perhaps a linear term in ω take place.

In our analysis, we consider the static spherically symmetric BH in effective loop quantum gravity and investigate its characteristics by computing its deflection angle, Hawking radiation and bounds of the greybody factor.

This paper is arranged as follows. In section **2**, we discuss about the BH in effective loop quantm gravity. In section **3**, we obtain the deflection angle of the BH and analyze its graphical behaviour in non-plasma medium. In section **4**, we compute the deflection angle of the BH and analyze its graphical behaviour in plasma medium. In section **5**, we examine the deflection angle of BH in dark matter medium. Section **6**, consists of the calculation of bending angle of BH utilizing Keeton and Petters method. In section **7**, we calculate the Hawking temperature via GBT. In section **8**, we calculate the bounds of the greybody factor of the BH and analyze their graphical behaviour. In section **9**, we conclude our results.

II. BLACK HOLE IN EFFECTIVE LOOP QUANTUM GRAVITY

The common properties of the BHs in loop quantum gravity are that the singularities within them are changed by a transition surface, which connects a BH to a white hole and that the spacetime is exact everywhere. The static spherically symmetric

Preprints (www.preprints.org) | NOT PEER-REVIEWED | Posted: 15 June 2022 doi:10.20944/preprints202206.0211.v1

metric after solving the effective equations of the loop quantum gravity and redefining the two new coordinates can be defined as [97]:

$$ds^2 = -A(r)dt^2 + B(r)dr^2 + C(r)(d\theta^2 + sin^2\theta d\phi^2), \tag{2}$$

where

$$A(r) = \frac{1}{B(r)} = \frac{\sqrt{8A_\lambda M^2 + r^2}(\sqrt{8A_\lambda M^2 + r^2} - 2M)}{2A_\lambda M^2 + r^2}, \tag{3}$$

$$C(r) = 2A_\lambda M^2 + r^2, \tag{4}$$

where A_λ is the dimensionless non-negative parameter. It can be observed that if $A_\lambda = 0$ and $M \neq 0$ metric represents a Schwarzschild BH, a regular BH when the value of A_λ is $0 < A_\lambda < \frac{1}{2}$, if $A_\lambda = \frac{1}{2}$ it represents a traversable wormhole with a null thorat and a wormhole with a two-way throat at $r = 0$. If $M = 0$ metric represents a flat spacetime.

III. DEFLECTION ANGLE IN NON-PLASMA MEDIUM

In this section, we determine the deflection angle $(\breve{\delta})$ of BH in non-plasma medium using GBT. In order to use the GBT, we obtain the optical metric by using Eq.(2) and just writing it into equatorial plane $(\theta = \frac{\pi}{2})$ to acquire the null geodesics $(ds^2 = 0)$ as

$$dt^2 = \frac{B(r)}{A(r)}dr^2 + \frac{C(r)}{A(r)}d\phi^2. \tag{5}$$

The non-zero Christoffel symbols of metric in (5) are calculated as

$$\Gamma^r_{rr} = \frac{1}{2}\left(-\frac{A'(r)}{A(r)} + \frac{B'(r)}{B(r)}\right),$$

$$\Gamma^r_{\phi\phi} = \frac{C(r)A'(r) - A(r)C'(r)}{2A(r)B(r)},$$

$$\Gamma^\phi_{r\phi} = \frac{1}{2}\left(-\frac{A'(r)}{A(r)} + \frac{C'(r)}{C(r)}\right). \tag{6}$$

The Gaussian optical curvature $\mathcal{K}$ is an intrinsic feature of spacetime, corresponding to the optical metric, which is associated to its Ricci scalar $\mathcal{R}$ i.e.,

$$\mathcal{K} = \frac{\mathcal{R}}{2}. \tag{7}$$

Using non-zero Christoffel symbols and Ricci scalar, Eq.(7) implies the following optical Gaussian curvature

$$\mathcal{K} \simeq \frac{-2M}{r^3} + \frac{(3 + 16A_\lambda)M^2}{r^4} + \mathcal{O}(M^3, A_\lambda^2). \tag{8}$$

Now, we calculate the deflection angle of the BH using GBT. Utilizing GBT in the non-singular domain $\mathcal{J}_R$, given as [20]:

$$\int\int_{\mathcal{J}_R} \mathcal{K}dS + \oint_{\partial\mathcal{J}_R} kd\sigma + \sum_j \tilde{\theta}_j = 2\pi\mathcal{X}(\mathcal{J}_R). \tag{9}$$

Here, $\tilde{\theta}_j$ is the external angle of j^{th} vertex and $\mathcal{X}(\mathcal{J}_R) = 1$ represents the Euler characteristic number and k indicates the geodesic curvature as well as it is determined as $k = \tilde{g}(\nabla_{\dot{\alpha}}\dot{\alpha}, \ddot{\alpha})$ [20], in such a way that $\tilde{g}(\dot{\alpha}, \dot{\alpha}) = 1$, where $\ddot{\alpha}$ denotes the unit acceleration vector. As $\mathcal{R} \to \infty$, the corresponding jump angles reduces to $\frac{\pi}{2}$ such that $\theta_o + \theta_T \to \pi$. So

$$\int\int_{\mathcal{J}_R} \mathcal{K}dS + \oint_{\partial\mathcal{J}_R} kd\sigma + \tilde{\theta}_j = 2\pi\mathcal{X}(\mathcal{J}_R), \tag{10}$$

Preprints (www.preprints.org) | NOT PEER-REVIEWED | Posted: 15 June 2022 doi:10.20944/preprints202206.0211.v1

where, $\tilde{\theta}_j = \pi$ indicates the entire jump angle. As $\mathcal{R} \to \infty$, the most useful element is to be obtained is

$$k(F_R) = \mid \nabla_{\dot{F}_R} \dot{F}_R \mid . \tag{11}$$

The radial component of the geodesic curvature is obtained as follows

$$(\nabla_{\dot{F}_R} \dot{F}_R)^r = \dot{F}_C^{\phi} \partial_{\phi} \dot{F}_R^r + \Gamma^r_{\phi\phi} (\dot{F}_R^{\phi})^2. \tag{12}$$

Taking into account $F_R = r(\phi) = R = constant$, we have

$$(\nabla_{\dot{F}_R^r} \dot{F}_R^r)^r \to \frac{-1}{R}. \tag{13}$$

It is stated that the geodesic curvature does now not depending upon on topological defects, so that $k(F_R) \to \frac{-1}{R}$. After a while, from the optical metric (5), one can obtain $dt = Rd\phi$, which implies

$$k(F_R)dt = \frac{1}{R} Rd\phi. \tag{14}$$

Using the above equations and the the straight line approximation $r = \frac{b}{sin\phi}$, where b represents the impact parameter, the deflection angle can be computed as:

$$\breve{\delta} = -\int_0^{\pi} \int_{b/\sin\phi}^{\infty} \mathcal{K} dS, \tag{15}$$

where, $dS = \sqrt{det\tilde{g}} dr d\phi$. Using the Eqs.(8) and (15), the bending angle $(\breve{\delta})$ can be calculated as

$$\breve{\delta} \simeq \frac{4M}{b} + \frac{3M^2\pi}{4b^2} - \frac{4A_{\lambda}M^2\pi}{b^2} + \mathcal{O}(M^3, A_{\lambda}^2). \tag{16}$$

The obtained deflection angle (16) depends on the mass of the BH, dimensionless non-negative parameter A_{λ} and the impact parameter b. The first and second terms in the deflection angle $(\breve{\delta})$ is similar to the deflection angle of the Schwarzschild BH upto second order of mass M. The third term in the deflection angle $(\breve{\delta})$ is due to the the quantum effects. While the negative sign with the third term represents the negative contribution of the quantum effects on the deflection angle. The deflection angle $(\breve{\delta})$ obtained in non-plasma medium converts into the deflection angle of Schwarzschild BH upto second order of mass M in non-plasma medium if we take $A_{\lambda} = 0$.

A. Graphical Analysis of Deflection Angle in Non-Plasma Medium

This subsection is mainly focus on the graphical study of BH's deflection angle $(\breve{\delta})$ in non-plasma medium for the distinct values of dimensionless non-negative parameter A_{λ}, by keeping $M = 1$ and choosing impact parameter $0 \leq b \leq 50$.

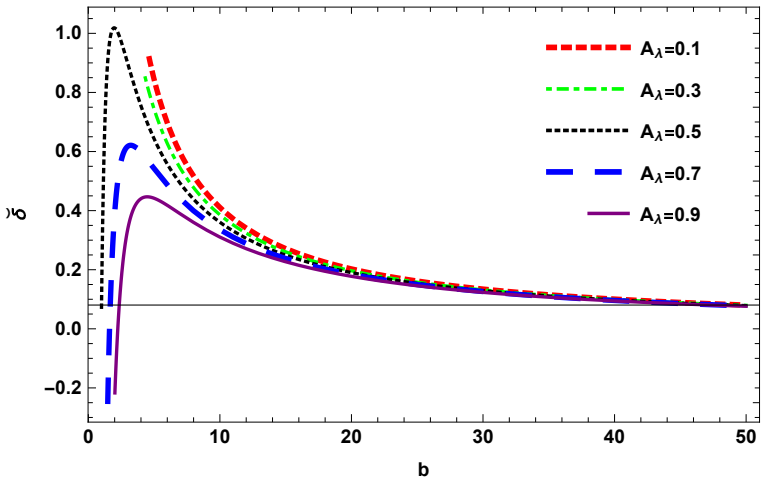

Figure 1: $\breve{\delta}$ versus b, $0 < A_{\lambda} < 1$.

Preprints (www.preprints.org) | NOT PEER-REVIEWED | Posted: 15 June 2022 doi:10.20944/preprints202206.0211.v1

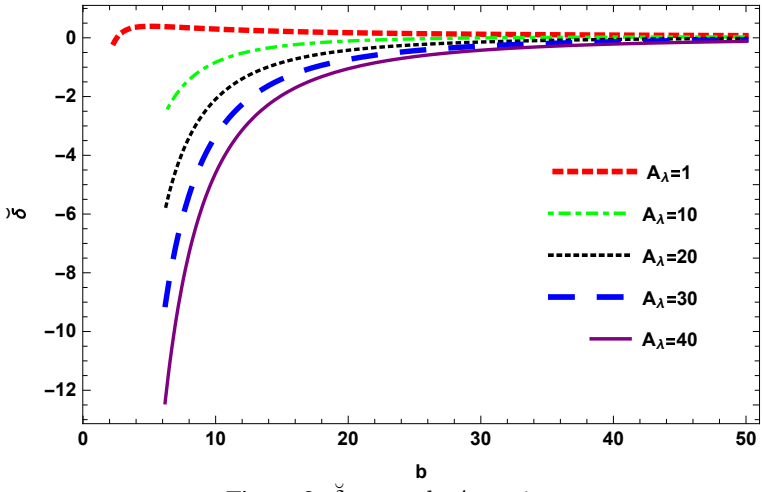

Figure 2: $\breve{\delta}$ versus b, $A_\lambda \geq 1$.

- For $0 < A_\lambda < 1$, **figure 1** shows the graphical behaviour of deflection angle $(\breve{\delta})$ versus impact parameter b. We find that the bending angle $(\breve{\delta})$ ranges from negative values to maximum values at small values of impact parameter b. As the value of impact parameter b increases, the deflection angle approaches to zero. We also examine that the deflection angle attains its maximum value as $A_\lambda \to 0$ and then exponentially decreases. For this range of small value of b and A_λ, one can obtain the maximum positive angle, which indicates that the deflection is upward. In this case, we can obtain the physically stable behaviour of deflection angle.

- For $A_\lambda \geq 1$, **figure 2** demonstrates the graphical behaviour of deflection angle $(\breve{\delta})$ versus impact parameter b. We analyze that initially the deflection angle $(\breve{\delta})$ exponentially approaches to zero. As A_λ decreases and approaches to its maximum values, the deflection angle approaches to zero from negative side. For $A_\lambda \geq 1$, one can obtain the negative angle, which represents that the deflection is downward. Physically the behaviour of the deflection angle in this range is also stable.

IV. DEFLECTION ANGLE IN PLASMA MEDIUM

This section aims to examine the impact of the plasma medium on the deflection angle $(\breve{\delta})$. The BH within plasma is explained by the refractive index [98, 99].

$$n(r) = \sqrt{1 - \frac{\omega_e^2}{\omega_\infty^2}(A(r))}, \tag{17}$$

where, ω_e^2 and ω_∞^2 stand for electron plasma frequency and photon frequency considered by an spectator at infinity, respectively. The corresponding optical metric is determined as:

$$d\sigma = g_{uv}^{opt} dx^u dx^v = n^2(r)\left[\frac{B(r)}{A(r)}dr^2 + \frac{C(r)}{A(r)}d\phi^2\right]. \tag{18}$$

The optical Gaussian curvature for the metric (18) is computed as

$$\mathcal{K} \simeq -\frac{2M}{r^3} - \frac{3M\omega_e^2}{r^3\omega_\infty^2} + \frac{(3+16A_\lambda)M^2}{r^4} + \frac{4(3+7A_\lambda)M^2\omega_e^2}{r^4\omega_\infty^2} + \mathcal{O}(M^3, A_\lambda^2). \tag{19}$$

By utilizing GBT, we acquire the deflection angle $(\breve{\delta})$ of BH within the plasma medium. Thus, for obtaining the deflection angle $(\breve{\delta})$ we apply the straight line approximation $r = \frac{b}{sin\phi}$ at the 0th order, we obtained

$$\breve{\delta} = -\int_0^\pi \int_{\frac{b}{\sin\phi}}^R \mathcal{K} dS, \tag{20}$$

Using Eq.(20), the deflection angle $(\breve{\delta})$ is calculated as:

$$\breve{\delta} \simeq \frac{4M}{b} + \frac{3M^2\pi}{4b^2} - \frac{4A_\lambda M^2\pi}{b^2} + \frac{2M\omega_e^2}{b\omega_\infty^2} - \frac{M^2\pi\omega_e^2}{2b^2\omega_\infty^2} - \frac{3A_\lambda M^2\pi\omega_e^2}{b^2\omega_\infty^2} + \mathcal{O}(M^3, A_\lambda^2). \tag{21}$$

Preprints (www.preprints.org) | NOT PEER-REVIEWED | Posted: 15 June 2022 doi:10.20944/preprints202206.0211.v1

The obtained deflection angle (21) depends on the mass of the BH, dimensionless non-negative parameter A_λ, impact parameter b and plasma term. One can see that the first three terms in the deflection angle (21) are same as in the angle (16). If we neglect the effect of plasma medium $\frac{\omega_e^2}{\omega_\infty^2} \to 0$, then the angle obtained in plasma medium reduces into the angle (16) that we obtained in non-plasma medium. We also observed that the deflection angle $(\breve{\delta})$ increases with the plasma term, which represents that by lowering the photon frequency observed by a static viewer at infinity, the deflection angle $(\breve{\delta})$ increases, keeping electron plasma frequency fixed. If we take $A_\lambda = 0$, then the obtained deflection angle reduces into the deflection angle of Schwarzschild BH upto second order of mass M in plasma medium.

A. Graphical Analysis of Deflection Angle in Plasma Medium

This subsection is devoted to study the graphical behaviour of BH's bending angle $(\breve{\delta})$ in plasma medium. We take $\frac{\omega_e}{\omega_\infty} = \frac{1}{10}$, $M = 1$ and impact parameter $0 \leq b \leq 50$ to analyze the graphical behaviour of bending angle $(\breve{\delta})$ versus impact parameter b for the different values of A_λ

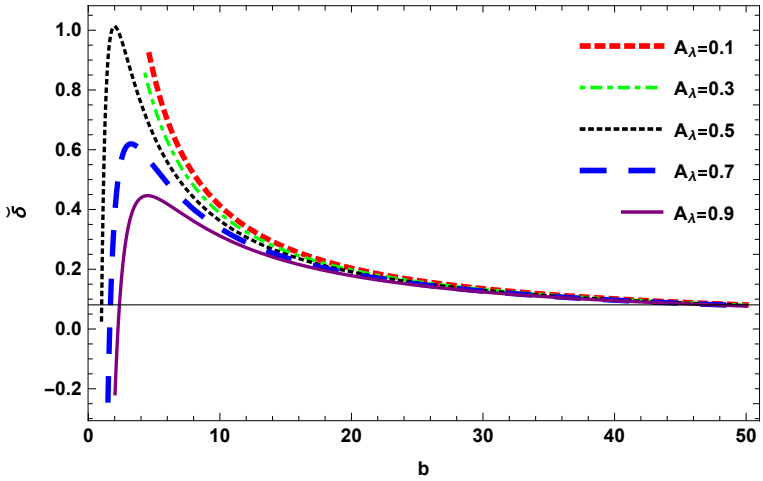

Figure 3: $\breve{\delta}$ versus b, $0 < A_\lambda < 1$.

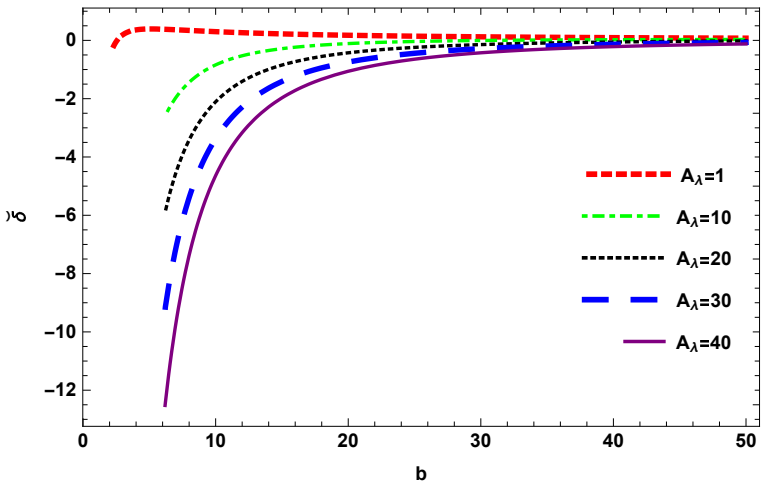

Figure 4: $\breve{\delta}$ versus b, $A_\lambda \geq 1$.

- For $0 < A_\lambda < 1$, **figure 3** exhibits the graphical behaviour of deflection angle $(\breve{\delta})$ versus impact parameter b. We find that the bending angle $(\breve{\delta})$ ranges from negative values to maximum values at small values of impact parameter b. As the value of impact parameter b increases, the deflection angle approaches to zero. We also examine that the deflection angle attains its maximum value as $A_\lambda \to 0$ and then exponentially decreases. For this range of small value of b and A_λ, one can obtain the maximum positive angle, which indicates that the deflection is upward. In this case, we can obtain the physically stable behaviour of deflection angle.

Preprints (www.preprints.org) | NOT PEER-REVIEWED | Posted: 15 June 2022 doi:10.20944/preprints202206.0211.v1

- For $A_\lambda \geq 1$, **figure 4** represent the graphical behaviour of deflection angle $(\breve{\delta})$ versus impact parameter b. We analyze that initially the deflection angle $(\breve{\delta})$ exponentially approaches to zero. As A_λ decreases and approaches to its maximum values, the deflection angle approaches to zero from negative side. For $A_\lambda \geq 1$, one can obtain the negative angle, which represents that the deflection is downward. Physically the behaviour of the deflection angle in this range is also stable.

We have determined that the bending angle $(\breve{\delta})$ exhibits same behaviour graphically in non-plasma and plasma mediums in terms of the positive and negative values of the deflection angle.

V. DARK MATTER MEDIUM EFFECT ON WEAK GRAVITATIONAL LENSING

This section focuses on the calculations of the deflection angle $(\breve{\delta})$ in dark matter medium using GBT. To achieve this, we utilize the refractive index for the dark matter medium which is defined as [96]:

$$n(\omega) = 1 + \beta A_0 + A_2\omega^2. \tag{22}$$

The Gaussian optical curvature in dark matter medium after using Eq.(7) and the value of n in Eq.(18) is calculated as

$$\mathcal{K} \approx -\frac{2M}{r^3(1+\beta A_0 + A_2\omega^2)^2} + \frac{(3+16A_\lambda)M^2}{r^4(1+\beta A_0 + A_2\omega^2)^2}. \tag{23}$$

Using Eq.(20), the deflection angle $(\breve{\delta})$ is obtained as follows

$$\begin{aligned}\breve{\delta} \approx\ & \frac{4M}{b(1+\beta A_0 + A_2\omega^2)^6} + \frac{3M^2\pi}{4b^2(1+\beta A_0 + A_2\omega^2)^6} - \frac{4A_\lambda M^2\pi}{b^2(1+\beta A_0 + A_2\omega^2)^6} \\ &+ \frac{24M\omega^2 A_2}{b(1+\beta A_0 + A_2\omega^2)^6} + \frac{9M^2\pi A_2\omega^2}{2b^2(1+\beta A_0 + A_2\omega^2)^6} \\ &- \frac{24A_\lambda M^2\pi A_2\omega^2}{b^2(1+\beta A_0 + A_2\omega^2)^6} + \mathcal{O}(\omega^4).\end{aligned} \tag{24}$$

The obtained deflection angle (24) depends on the mass of the BH, dimensionless non-negative parameter A_λ and the impact parameter b. If we take $A_\lambda = 0$ in Eq.(24), then the obtained deflection angle reduces into the deflection angle of Schwarzschild BH upto second order of mass M in dark matter medium. We also observed that the bending angle in case of dark matter medium is larger than in general. If we remove the influence of dark matter medium, then the deflection angle reduces into the deflection angle that we obtained in the non-plasma medium.

VI. DEFLECTION ANGLE BY USING KEETON AND PETTERS METHOD

This section consists on the calculations of the bending angle $(\breve{\delta})$ of BH using Keeton and Petters technique [100]. In a generic asymptotically flat metric theory of gravity, Keeton and Petters constructed a highly helpful framework for computing corrections to a core set of observable characteristics. The goal is to show how to use post-post-Newtonian (PPN) correction terms up to third order to address lensing in alternative gravity theories. Their technique allows researchers to calculate observable values that are basically coordinate independent and hence physically meaningful.

For this, first we convert the metric into standard form. The static spherically symmetric metric (2) after putting the values of the metric functions is defined as:

$$\begin{aligned}ds^2 =\ & -\left(\frac{\sqrt{8A_\lambda M^2 + r^2}(\sqrt{8A_\lambda M^2 + r^2} - 2M)}{2A_\lambda M^2 + r^2}\right) dt^2 \\ &+ \left(\frac{\sqrt{8A_\lambda M^2 + r^2}(\sqrt{8A_\lambda M^2 + r^2} - 2M)}{2A_\lambda M^2 + r^2}\right)^{-1} dr^2 \\ &+ r^2\left(1 + \frac{2A_\lambda M^2}{r^2}\right)(d\theta^2 + sin^2\theta d\phi^2).\end{aligned} \tag{25}$$

Dividing the metric by $\left(1 + \frac{2A_\lambda M^2}{r^2}\right)$ and setting the metric functions equal to $G(r)$ and $H(r)$, we get the standard form of the metric defined as:

$$ds^2 = -G(r)dt^2 + H(r)dr^2 + r^2 d\Omega^2, \tag{26}$$

Preprints (www.preprints.org) | NOT PEER-REVIEWED | Posted: 15 June 2022 doi:10.20944/preprints202206.0211.v1

where

$$G(r) = \frac{1}{H(r)} = \frac{\sqrt{8A_\lambda M^2 + r^2}(\sqrt{8A_\lambda M^2 + r^2} - 2M)}{(2A_\lambda M^2 + r^2)\left(1 + \frac{2A_\lambda M^2}{r^2}\right)} \tag{27}$$

and

$$d\Omega^2 = d\theta^2 + \sin^2\theta d\phi^2. \tag{28}$$

Following the Keeton and Petters technique [100], the coefficients of the standard metric (26) upto third order in PPN series are written as

$$G(r) = 1 + 2g_1\left(\frac{\phi}{c^2}\right) + 2g_2\left(\frac{\phi}{c^2}\right)^2 + 2g_3\left(\frac{\phi}{c^2}\right)^3 + ...$$

$$H(r) = 1 - 2h_1\left(\frac{\phi}{c^2}\right) + 4h_2\left(\frac{\phi}{c^2}\right)^2 - 8h_3\left(\frac{\phi}{c^2}\right)^3 + ..., \tag{29}$$

where ϕ which is the 3-dimensional Newtonian potential

$$\frac{\phi}{c^2} = -\frac{M}{r}. \tag{30}$$

Now we expand the metric function as a Taylor series in $\left(\frac{M}{r}\right)$

$$G(r) \approx 1 - \frac{2M}{r} + \frac{4A_\lambda M^2}{r^2} + \mathcal{O}\left(\frac{M^4}{r^4}\right). \tag{31}$$

$$\begin{aligned} H(r) \;&\approx\; 1 + \frac{2M}{r} - \frac{4(A_\lambda - 1)M^2}{r^2} - \frac{8(2A_\lambda - 1)M^3}{r^3} \\ &+\; \mathcal{O}\left(\frac{M^4}{r^4}\right). \end{aligned} \tag{32}$$

By comparing the coefficients of the expanded form of metric functions with the PPN coefficients in Eq.(29), we obtain

$$\begin{aligned} g_1 &= 1 \qquad g_2 = 2A_\lambda \qquad g_3 = 0, \\ h_1 &= 1 \qquad h_2 = -(A_\lambda - 1) \quad h_3 = -(2A_\lambda - 1). \end{aligned} \tag{33}$$

The expanded form of the deflection angle $(\breve{\delta})$ is defined as:

$$\breve{\delta} = A_1\left(\frac{M}{b}\right) + A_2\left(\frac{M^2}{b^2}\right) + A_3\left(\frac{M^3}{b^3}\right) + \mathcal{O}\left(\frac{M^4}{b^4}\right). \tag{34}$$

Where the coefficients of expanded form of the deflection angle are defined as:

$$\begin{aligned} A_1 &= 2(g_1 + h_1), \\ A_2 &= \left(2g_1^2 - g_2 + g_1h_1 - \frac{h_1^2}{4} + h_2\right)\pi, \\ A_3 &= \frac{2}{3}\left(35g_1^3 + 15g_1^2h_1 - 3g_1(10g_2 + h_1^2 - 4h_2) + 6g_3\right. \\ &+\; \left. h_1^3 - h_1^3 - 6g_2h_1 - 4h_1h_2 + 8h_3\right). \end{aligned} \tag{35}$$

Now, we determine the coefficients of expanded form of the deflection angle $\breve{\delta}$ by using the Eq.(35) as

$$\begin{aligned} A_1 &= 4, \\ A_2 &= \frac{15\pi}{4}, \\ A_3 &= \frac{128}{3} - \frac{192A_\lambda}{3}. \end{aligned} \tag{36}$$

Preprints (www.preprints.org) | NOT PEER-REVIEWED | Posted: 15 June 2022 doi:10.20944/preprints202206.0211.v1

The deflection angle $(\breve{\delta})$ can be obtained by putting the values of the coefficients in 34

$$\breve{\delta} = \left(\frac{4M}{b}\right) + \left(\frac{15\pi M^2}{4b^2}\right) + \left(\frac{(128 - 192A_\lambda)M^3}{3b^3}\right) + \mathcal{O}\left(\frac{M^4}{b^4}\right). \tag{37}$$

The obtained deflection angle using Keeton and Petters technique depends on the mass of the BH, dimensionless non-negative parameter A_λ and the impact parameter b. The obtained angle (37) reduces to the deflection angle of the Schwarzschild BH using Keeton and Petters technique [100], when $A_\lambda = 0$.

VII. HAWKING RADIATION

This section is mainly focus on the calculations of the Hawking temperature by applying GBT. This topological technique calculates the BH temperature by using 2-dimensional Euler characteristic and GBT [64, 65]. For this purpose, static spherically symmetric metric is defined as

$$ds^2 = -G(r)dt^2 + H(r)dr^2 + r^2(d\theta^2 + sin^2\theta d\phi^2), \tag{38}$$

where

$$G(r) = \frac{1}{H(r)} = \frac{\sqrt{8A_\lambda M^2 + r^2}(\sqrt{8A_\lambda M^2 + r^2} - 2M)}{(2A_\lambda M^2 + r^2)\left(1 + \frac{2A_\lambda M^2}{r^2}\right)}. \tag{39}$$

Using Wick rotation condition, one can obtain the following 2-dimensional Euclidean metric

$$ds^2 = -G(r)dt^2 + \frac{1}{G(r)}dr^2. \tag{40}$$

The event horizon of the BH is obtained as follows

$$r_h = 2\sqrt{M^2 - 2A_\lambda M^2}, \tag{41}$$

while the Ricci scalar is obtained as

$$\begin{aligned}
\mathcal{R} &= \frac{4M(-1024A_\lambda^5 M^9(-4M + \Psi) + r^8(r^2 - 2M\Psi))}{(2A_\lambda M^2 + r^2)^4(8A_\lambda M^2 + r^2)^2(\Psi)} \\
&- \frac{512A_\lambda M^8(101Mr^2 + 4M^2\Psi - 24r^2\Psi)}{(2A_\lambda M^2 + r^2)^4(8A_\lambda M^2 + r^2)^2(\Psi)} \\
&+ \frac{16A_\lambda^2 M^4 r^4(53Mr^2 + 18M^2\Psi - 11r^2\Psi) - 8A_\lambda M^2 r^6(-20Mr^2 + 20M^2\Psi + 3r^2\Psi)}{(2A_\lambda M^2 + r^2)^4(8A_\lambda M^2 + r^2)^2(\Psi)} \\
&+ \frac{32A_\lambda^3 M^6 r^2(-127Mr^2 + 110M^2\Psi + 27r^2\Psi)}{(2A_\lambda M^2 + r^2)^4(8A_\lambda M^2 + r^2)^2(\Psi)}.
\end{aligned} \tag{42}$$

where $\Psi = \sqrt{8A_\lambda M^2 + r^2}$. The formula to calculate the Hawking temperature of the BH is written as follows

$$T_H = \frac{1}{4\pi\mathcal{X}} \int_{r_h} \sqrt{g}\mathcal{R}dr, \tag{43}$$

where $\mathcal{X} = 1$ is the Euler characteristic and g is the determinant. After putting the values of g and $\mathcal{R}$ and evaluating the integral (43), we get the Hawking Temperature of BH as

$$T_H = \frac{(1 - 2A_\lambda)^{3/2}}{2(2 - 3A_\lambda)^2 M\pi}. \tag{44}$$

The Hawking temperature (44) depends on the mass of the BH and dimensionless non-negative parameter A_λ. If we put $A_\lambda = 0$ in (44) then the obtained Hawking temperature of the BH reduces to the Hawking temperature of the Schwarzschild BH defined as $T_H = \frac{1}{8M\pi}$. Now, we also observe that the obtained Hawking Temperature using GBT is same as the standard form of the Hawking temperature at horizon $(T_H = \frac{f'(r_h)}{2\pi})$.

Preprints (www.preprints.org) | NOT PEER-REVIEWED | Posted: 15 June 2022 doi:10.20944/preprints202206.0211.v1

VIII. GREYBODY BOUNDS

In this section, we determine the fermionic rigorous bounds on the greybody factor [101]. The static spherically symmetric metric is defined in (38). The rigorous bound on the greybody factor is defined as

$$T \geq \text{sech}^2\left(\int_{-\infty}^{\infty} \eth dr_*\right). \tag{45}$$

where

$$\eth = \frac{\sqrt{[f'(r_*)]^2 + [\omega^2 - V(r_*) - f^2(r_*)]^2}}{2f(r_*)} \tag{46}$$

and $f(r_*)$ is a positive function which satisfies $f(-\infty) = f(\infty) = \omega$ [84]. Accordingly,

$$T \geq \text{sech}^2\left(\frac{1}{2\omega}\int_{-\infty}^{\infty} \mid \hat{V} \mid dr_*\right), \tag{47}$$

is in the the tortoise coordinate, where r_* is

$$\frac{dr_*}{dr} = \frac{G}{d}, \quad \text{where} \quad d = 1 + \frac{Gm\nu}{2\omega(m^2r^2 + \nu^2)}, \tag{48}$$

where, $\nu = \pm 1, \pm 2, \pm 3, ...$ are the eigenvalues of the angular part. The potential $\hat{V}_\pm$ can be defined as

$$\hat{V}_\pm = \pm\frac{dU}{dr_*} + U^2, \quad \text{where} \quad U = \frac{c}{d} \quad \text{and} \quad c = \frac{\sqrt{G}\sqrt{\nu^2 + m^2r^2}}{r}. \tag{49}$$

There value of U can be defined as

$$U = \frac{(\sqrt{G}/r)\sqrt{\nu^2 + m^2r^2}}{1 + (1/2\omega)G(r)[\nu m/(\nu^2 + m^2r^2)]}. \tag{50}$$

Substituting the value of the potential from Eq.(50) in (47), we get

$$T \geq \text{sech}^2\left(\frac{1}{2\omega}\int_{-\infty}^{\infty} \left|\pm\frac{dU}{dr_*} + U^2\right| dr_*\right). \tag{51}$$

After simplification,

$$T_b = T \geq \text{sech}^2\left(\frac{1}{2\omega}\int_{-\infty}^{\infty} \left|\pm\frac{dU}{dr_*}\right| dr_* + \frac{1}{2\omega}\int_{-\infty}^{\infty} \left|U^2\right| dr_*\right). \tag{52}$$

Let us examine one by one first and the second integrals in Eq.(52). By solving the first integral, we get

$$\int_{-\infty}^{\infty} \left|\pm\frac{dU}{dr_*}\right| = U\,|_{r=r_+}^{r=r_-} = 0. \tag{53}$$

where r_+ and r_- are the two real horizons of the BH. After evaluating the second integral in (52) we get the following expression

$$\int_{-\infty}^{\infty} \left|U^2\right| dr_* = \int_{r_+}^{r_-} \frac{(\nu^2 + m^2r^2)^2}{(r^2(\nu^2 + m^2r^2 + (\nu\omega) \mid G(r) \mid))} dr. \tag{54}$$

The outcomes of this formulation is considerably distinct among the massless and the massive instances. So, we separately consider these two cases.

We put $m = 0$ for the massless case in (54) then the integral can be written as

$$\int_{-\infty}^{\infty} \left|U^2\right| dr_* = \int_{r_+}^{r_-} \frac{\nu^2}{r^2} dr = \nu^2\left(\frac{1}{r_+} - \frac{1}{r_-}\right). \tag{55}$$

Preprints (www.preprints.org) | NOT PEER-REVIEWED | Posted: 15 June 2022 doi:10.20944/preprints202206.0211.v1

By putting the result obtained in Eq.(55) in (52), the rigorous bond can be calculated as

$$T_b = \text{sech}^2\left(\frac{\nu^2}{2\omega}\left[\frac{1}{r_+}-\frac{1}{r_-}\right]\right). \tag{56}$$

The two real horizons of the BH are defined as follows

$$r_+ = 2\sqrt{M^2-2A_\lambda M^2} \quad \text{and} \quad r_- = -2\sqrt{M^2-2A_\lambda M^2}. \tag{57}$$

The rigorous bond of the BH in the case of massless fermion after putting the values of the horizons in Eq.(56) is calculated as

$$T_b = \text{sech}\left[\frac{\nu^2}{2\omega}\left[\frac{1}{\sqrt{M^2-2A_\nu M^2}}\right]\right]^2. \tag{58}$$

Now, for the massive case, integral in (54) can be computed as

$$\int_{-\infty}^{\infty}\left|U^2\right|dr_* = \int_{r_+}^{r_-}\frac{\nu^2(1+\mu^2r^2)}{r^2\left(1+\frac{G\mu}{2\omega(\mu^2r^2+1)}\right)}. \tag{59}$$

Here, $\mu = \frac{m}{\nu}$, and we can also write $C = \frac{\nu^2(1+\mu^2r^2)}{r^2\left(1+\frac{G\mu}{2\omega(\mu^2r^2+1)}\right)}$, then Eq.(59) becomes

$$\int_{-\infty}^{\infty}\left|U^2\right|dr_* = \int_{r_+}^{r_-}Cdr, \tag{60}$$

By taking the above equation into consideration, we observe that the factor $C = \frac{\nu^2(1+\mu^2r^2)}{r^2\left(1+\frac{G\mu}{2\omega(\mu^2r^2+1)}\right)} > 1$. Using this inequality, we approximate the integrand, which can be written as

$$C = \frac{\nu^2(1+\mu^2r^2)}{r^2\left(1+\frac{G\mu}{2\omega(\mu^2r^2+1)}\right)} \leq \frac{\nu^2(1+\mu^2r^2)}{r^2} = C_{app}. \tag{61}$$

Here, C and C_{app} are the positive functions when $r_+ < r < r_-$, and the integral can be written as

$$T_b = T \geq \text{sech}^2\left(\int_{r_+}^{r_-}C_{app}dr\right). \tag{62}$$

After putting the value of C_{app} in the above expression and after solving the integral, the greybody bound is obtained as

$$T_b = \text{sech}^2\left[\left(\frac{\nu^2}{2\omega}\frac{(r_- - r_+)}{r_-r_+}\left[1+\mu^2r_+r_-\right]\right)\right]. \tag{63}$$

The rigorous greybody bound in the case of massive fermions by putting the values of the horizons can be obtained as given below

$$T_b = \text{sech}^2\left[\frac{\nu^2\frac{1}{\sqrt{M^2-2A_\lambda M^2}}\left[1-4\left(M^2-2A_\lambda M^2\right)\mu^2\right]}{2\omega}\right]. \tag{64}$$

The obtained rigorous bounds for the massless and massive particles depends on the mass of the BH and dimensionless non-negative parameter A_λ. We observed that the obtained rigorous bounds in both massless and massive cases depend on the distance between the two horizons. Also we noticed that if the distance between the horizons decreases than the bound on the greybody factor increases. We also investigated that the rigorous bound for the greybody factor in the case of massive fermions is converted into the case of massless fermions when $\mu \to 0$.

Preprints (www.preprints.org) | NOT PEER-REVIEWED | Posted: 15 June 2022 doi:10.20944/preprints202206.0211.v1

A. Graphical Analysis of the Bounds on the Greybody Factor

This section is based on the discussion of the graphical behaviour of the rigorous bounds for the greybody factor for both cases massive fermions and massless fermions with respect to the ω, varying dimensionless non-negative parameter A_λ, while keeping fixed μ, ν and $M = 1$.

- **Massless fermions**

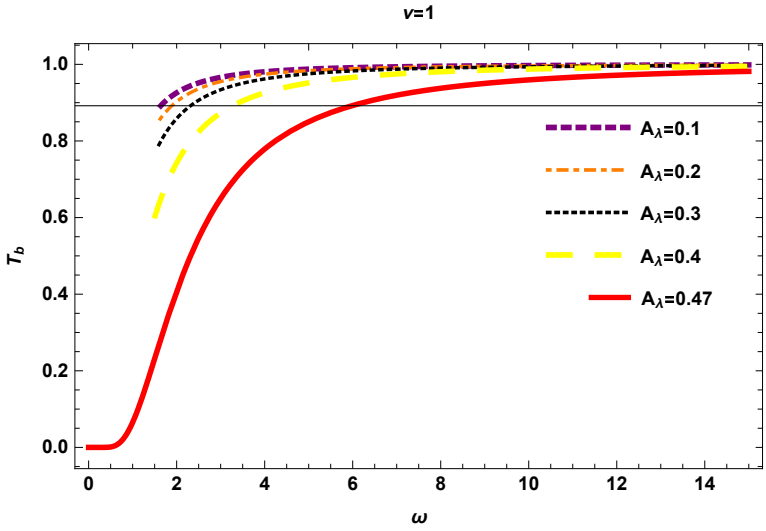

Figure 5: T_b versus ω, $0 < A_\lambda < 0.5$.

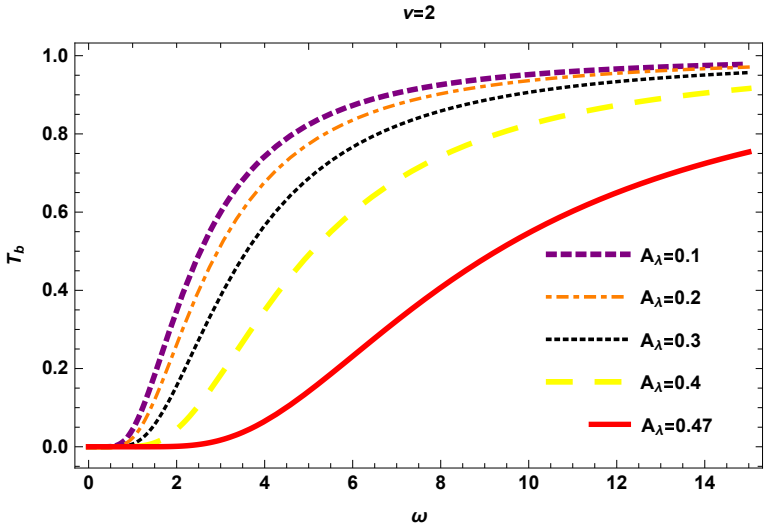

Figure 6: T_b versus ω, $0 < A_\lambda < 0.5$.

- For $\nu = 1$, **figure 5** shows the graphical behaviour of greybody factor bound T_b versus ω. We analyze that the bound T_b gradually decreasing as the value of A_λ increases. Moreover, as the value of ω increases the bound T_b shows the convergent behaviour and converges to the 1.

- For $\nu = 2$, **figure 6** depicts the graphical behaviour of greybody factor bound T_b versus ω. We notice that initially the bound T_b gradually decreases but as the value of A_λ increases the bound T_b rapidly decreases.

- **Massive fermions**

Preprints (www.preprints.org) | NOT PEER-REVIEWED | Posted: 15 June 2022 doi:10.20944/preprints202206.0211.v1

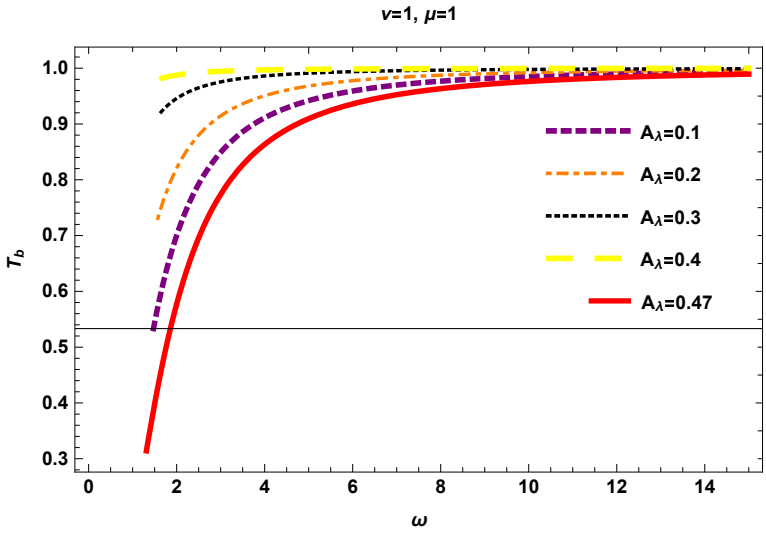

Figure 7: T_b versus ω, $0 < A_\lambda < 0.5$.

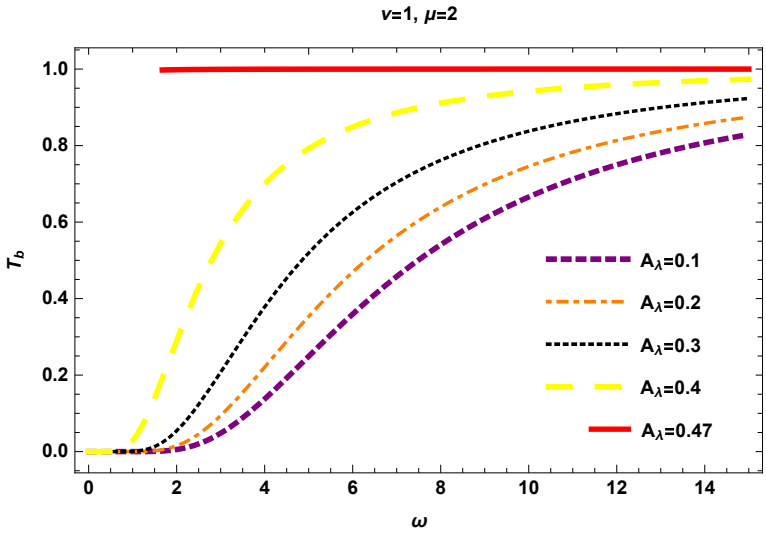

Figure 8: T_b versus ω, $0 < A_\lambda < 0.5$.

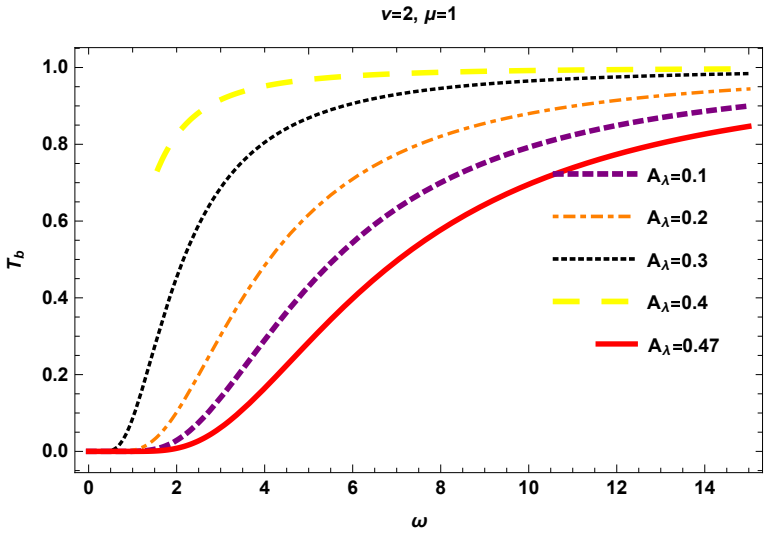

Figure 9: T_b versus ω, $0 < A_\lambda < 0.5$.

- For $\mu = \nu$, **figure 7** indicates the graphical behaviour of greybody factor bound T_b versus ω. We analyze that the bound T_b decreases as the value of A_λ increases. Moreover, as the value of ω increases the bound T_b approaches to 1.

Preprints (www.preprints.org) | NOT PEER-REVIEWED | Posted: 15 June 2022 doi:10.20944/preprints202206.0211.v1

- For $\mu > \nu$, **figure 8** shows the graphical behaviour of greybody factor bound T_b versus ω. We examine that when $\mu > \nu$ then the bound T_b steadily increasing when $0.1 \leq A_\lambda \leq 0.3$. As A_λ approaches to 0.5, the bound T_b rapidly increases and becomes constant. Also, the bound T_b shows the convergent behaviour and converges to 1.
- For $\nu > \mu$, **figure 9** indicates the graphical behaviour of greybody factor bound T_b versus ω. We observe that when $\nu > \mu$ the bound T_b increases as the value of A_λ increases. In this case, the bound T_b also shows the convergent behaviour.

IX. CONCLUSIONS

In this paper, we have discussed about the BH in effective loop quantum gravity and worked out the deflection angle $(\breve{\delta})$ of BH in non-plasma (16), plasma (21) and dark matter (24) mediums by using Gibbons and Werner technique. We have observed that the bending angle in these mediums depends on the mass M of the BH, impact parameter b and dimensionless non-negative parameter A_λ. We have also noticed that the contribution of the quantum effects on the deflection angle is negative. It is discussed that the obtained angle in these mediums reduces into the defection angle of the Schwarzschild BH upto the second order of mass M if we consider the dimensionless non-negative parameter $A_\lambda = 0$.

In case of **plasma medium**, the effect of the plasma increases the deflection angle. It is observed that the bending angle in plasma medium increases by lowering the photon frequency observed by a static viewer at infinity, by keeping electron plasma frequency fixed. While, it is to be noted that by neglecting the plasma term the obtained deflection angle (21) reduces to the non-plasma deflection angle (16). In case of **dark matter medium**, the bending angle in this medium is larger than non-plasma medium. After neglecting the influence of the dark matter medium, the obtained deflection angle (24) reduces to the non-plasma deflection angle (16).

Using Keeton and Petters technique, the obtained deflection angle (37) depends on the mass of the BH, dimensionless non-negative parameter A_λ and the impact parameter b. This deflection angle reduces to the angle of the Schwarzschild BH which is obtained by using Keeton and Petters technique, when $A_\lambda = 0$.

Furthermore, graphically we have determined that the deflection angle shows the similar graphical behaviour in both non-plasma and plasma mediums. For this purpose, we have analyzed the deflection angle $(\breve{\delta})$ with respect to the impact parameter b for the different values of A_λ and $M = 1$. For $0 < A_\lambda < 1$, the bending angle $(\breve{\delta})$ ranges from negative values to maximum values at small values of impact parameter b. As the value of impact parameter b increases, the deflection angle approaches to zero. We also examined that the deflection angle attains its maximum value as $A_\lambda \to 0$ and then exponentially decreases. We also marked that for this range of small value of b and A_λ, one can obtain the maximum positive angle, which indicates that the deflection is upward. For $A_\lambda \geq 1$, we noticed that the deflection angle $(\breve{\delta})$ exponentially approaches to zero. As A_λ decreases and approaches to its maximum values, the deflection angle approaches to zero from negative side. For $A_\lambda \geq 1$, one can obtain the negative angle, which represents that the deflection is downward. It is to be mentioned that physically the behaviour of the deflection angle in both cases is stable.

We have also investigated the **Hawking temperature** of the BH by using the GBT and observed that the obtained temperature is similar to the standard form of the Hawking temperature at horizon of a BH ($T_H = \frac{f'(r_h)}{2\pi}$). The Hawking temperature (44) depends on the mass of the BH and dimensionless non-negative parameter A_λ. If we put $A_\lambda = 0$, the Hawking temperature of the Schwarzschild BH $T_H = \frac{1}{8M\pi}$ is obtained.

Moreover, we have calculated the **fermonic greybody bounds** and discussed it for both cases massless and massive fermions separately. We observed that the obtained rigorous bounds (58) and (64) depend on the mass of the BH and dimensionless non-negative parameter A_λ. Later, we observed that the bounds obtained in the both cases depends on the distance between the two horizons and when the distance between the horizons decreases then the greybody factor bound increases. We also studied that the bound obtained in the massive case converts into the bound obtained in the massless case if $\mu \to 0$.

Lastly, we discussed the graphical behaviour of the greybody bound by fixing $M = 1$, giving different values to the A_λ, μ and ν. We noticed that in case of **massless fermions**, for $\nu = 1$ with $0 < A_\lambda < 0.5$, the bound T_b gradually decreasing. Moreover, as the value of ω increases the bound T_b shows the convergent behaviour and converges to the 1. For $\nu = 2$ with $0 < A_\lambda < 0.5$, We notice that initially the bound T_b gradually decreases but as the value of A_λ increases the bound T_b rapidly decreases. In case of **massive fermions**, we discussed three cases of μ and ν with $0 < A_\lambda < 0.5$ i.e. (i) $\mu = \nu$, (ii) $\mu > \nu$ and (iii) $\nu > \mu$. In $\mu = \nu$, the bound T_b decreases as the value of A_λ increases. Further, we observed that as the value of ω increases the bound T_b approaches to 1. For $\mu > \nu$, the bound T_b steadily increasing when $0.1 \leq A_\lambda \leq 0.3$ and as A_λ approaches to 0.5, the bound T_b rapidly increases and becomes constant. Also, we marked that the bound T_b shows the convergent behaviour and converges to 1 and for the case $\nu > \mu$, the bound T_b increases as the value of A_λ increases. In this case, the bound T_b also shows the convergent

behaviour.

[1] K. Akiyama *et al.*[Event Horizon Telescope Collaboration], Astrophys. J. **875**, no. 1, L1 (2019).
[2] F. Atamurotov, A. Abdujabbarov and B. Ahmedov, Phys. Rev. D **88**, 064004 (2013).
[3] R. A. Konoplya, Phys. Lett. B **795**, 1-6 (2019).
[4] C. Bambi, K. Freese, S. Vagnozzi and L. Visinelli, Phys. Rev. D **100**, 044057 (2019).
[5] R. Shaikh, Phys. Rev. D **100**, 024028 (2019).
[6] A. Abdujabbarov, B. Ahmedov, N. Dadhich and F. Atamurotov, Phys. Rev. D **96**, no. 8, 084017 (2017).
[7] A. Abdujabbarov, M. Amir, B. Ahmedov and S. G. Ghosh, Phys. Rev. D **93**, no. 10, 104004 (2016).
[8] E. F. Eiroa, G. E. Romero and D. F. Torres, Phys. Rev. D **66**, 024010 (2002).
[9] C. R. Keeton, C. S. Kochanek and E. E. Falco, Astrophys. J. **509**, 561-578 (1998).
[10] M. Sharif and S. Iftikhar, Astrophys. Space Sci. **361**, no.1, 36 (2016).
[11] K. S. Virbhadra, D. Narasimha and S. M. Chitre, Astron. Astrophys. **337**, 1-8 (1998).
[12] A. F. Zakharov, Int. J. Mod. Phys. D **27**, no.06, 1841009 (2018).
[13] K. S. Virbhadra and G. F. R. Ellis, Phys. Rev. D **65**, 103004 (2002).
[14] M. Bartelmann, Class. Quant. Grav. 27, 233001 (2010).
[15] R. Keeton, C. S. Kochanek and E. E. Falco, Astrophys. J. **509**, 561 (1998).
[16] A. Bhadra, Phys. Rev. D **67**, 103009 (2003).
[17] R. Whisker, Phys. Rev. D **71**, 064004 (2005).
[18] S. b. Chen and J. l. Jing, Phys. Rev. D **80** 024036, (2009).
[19] K. K Nandi, Y. Z. Zhang and A. V. Zakharov, Phys. Rev. D **74**, 024020 (2006).
[20] G. W. Gibbons and M. C. Werner, Class. Quant. Grav. **25**, 235009 (2008).
[21] M. C. Werner, Gen. Rel. Grav. **44**, 3047 (2012).
[22] K. Jusufi, I. Sakalli and A. Övgün, Phys. Rev. D **96**, 024040 (2017).
[23] Z. Li and A. Övgün, Phys. Rev. D **101(2)**, 024040 (2020).
[24] K. Jusufi and A. Övgün, Phys. Rev. D **97**, 024042 (2018).
[25] W. Javed, R. Babar and A. Övgün, Phys. Rev. D **99**, 084012 (2019).
[26] W. Javed, R. Babar and A. Övgün, Phys. Rev. D **100**, 104032 (2019).
[27] W. Javed, J. Abbas and A. Övgün, Phys. Rev. D **100(4)**, 044052 (2019).
[28] W. Javed, J. Abbas and A. Övgün, Eur. Phys. J. C **79**, 694 (2019).
[29] A. Ishihara, Y. Suzuki, T. Ono, T. Kitamura and H. Asada, Phys. Rev. D **94(8)**, 084015 (2016).
[30] A. Övgün, K. Jusufi and I. Sakalli, Ann. Phys. **399**, 193-203(2018).
[31] K. Jusufi and A. Övgün, Phys. Rev. D **97**, no.6, 064030(2018).
[32] A. Övgün, Phys. Rev. D **99**, no.10, 104075(2019).
[33] I. Sakalli and A. Ovgun, EPL 118, no.**6**, 60006(2017).
[34] K. de Leon and I. Vega, Phys. Rev. D **99**, no.12, 124007(2019).
[35] A. Övgün, I. Sakalli and J. Saavedra, Ann. Phys. **411**, 167978(2019).
[36] A. Övgün, I. Sakalli and J. Saavedra, JCAP **10**, 041(2018).
[37] T. Ono, A. Ishihara and H. Asada, Phys. Rev. D **98**, no.4, 044047(2018).
[38] K. Jusufi and A. Övgün, Int. J. Geom. Meth. Mod. Phys. **16**, no. 08, 1950116 (2019).
[39] Y. Kumaran and A. Övgün, Chin. Phys. C **44**, no.2, 025101 (2020)
[40] Z. Li, G. Zhang and A. Övgün, Phys. Rev. D **101**, no.12, 124058(2020).
[41] K. Jusufi, A. Övgün and A. Banerjee, Phys. Rev. D **96**, no.8, 084036(2017).
[42] K. Jusufi, A. Övgün, J. Saavedra, Y. Vasquez and P. A. Gonzalez, Phys. Rev. D **97**, no.12, 124024(2018).
[43] A. Övgün, K. Jusufi and I. Sakalli, Phys. Rev. D **99**, no.2, 024042(2019).
[44] K. Jusufi, A. Övgün, A.Banerjee and I. Sakalli, Eur. Phys. J. Plus **134**, no.9, 428 (2019).
[45] A. Övgün, G. Gyulchev and K. Jusufi, Ann. Phys. **406**, 152-172(2019).
[46] A. Övgün, Universe **5**, 115 (2019).
[47] A. Övgün, Phys. Rev. D **98**, no.4, 044033(2018).
[48] R. C. Pantig, P. K. Yu, E. T. Rodulfo and A. Övgün, Annals of Physics **436**, 168722 (2022).
[49] R. C. Pantig and A. Övgün, Eur. Phys. J. C **82**, no.5, 391 (2022).
[50] R. C. Pantig and E. T. Rodulfo, Chin. J. Phys. **66**, 691-702 (2020).
[51] W. Javed, R. Babar, and A. Övgün, Phys. Rev. D **99**, 084012(2019).
[52] W. Javed, A. Hazma and A. Övgün, Phys. Rev. D **101**, no.10, 103521 (2020).
[53] W. Javed, M. B. Khadim and A. Övgün, Eur. Phys. J. Plus **135**, 595 (2020).
[54] W. Javed, A. Hamza and A. Övgün, Mod. Phys. Lett. A **35**, no. 39, 2050322 (2020).
[55] W. Javed, A. Hamza and A. Övgün, Universe **7** ,10, 385 (2021).
[56] S. W. Hawking, Comm. Math. Phys. **43** 199 (1975).
[57] S. W. Hawking, Nature **248**, 30 (1974).
[58] G. W. Gibbons, S. W. Hawking, Phys. Rev. D **15**, 2738 (1977).

 doi:10.20944/preprints202206.0211.v1

[59] W. G. Unruh, Phys. Rev. D **14**, 870 (1976).
[60] T. Damour and R. Ruffini, Phys. Rev. D **14**, 332 (1976).
[61] M. K. Parikh and F. Wilczek, Phys. Rev. Lett. **85**, 5042 (2000).
[62] K. Srinivasan and T. Padmanabhan, Phys. Rev. D **60**, 024007 (1999).
[63] G. W. Gibbons and S. W. Hawking, Phys. Rev. D **15**, 2752 (1977).
[64] C. W. Robson, L. D. M. Villari and F. Biancalana, Phys. Rev. D **99 (4)** ,044042 (2019).
[65] C. W. Robson, L. D. M. Villari and F. Biancalana, arXiv:1902.02547 [gr-qc].
[66] A. Övgün and I. Sakalli, Ann. Phys. **413**, 168071 (2020).
[67] S. Fernando, Gen. Relativ. Gravit. **37**, 461-481 (2005).
[68] W. Kim and J. J. Oh, JKPS **52**, 986 - 991 (2008).
[69] J. Escobedo, Master's Thesis, Uni. of Amsterdam 6 (2008).
[70] M. K. Parikh and F. Wilczek, Phys. Rev. Lett. **85**, 5042-5045 (2000).
[71] P. Lange, thesis, Uppsala Universitet (2007).
[72] S. Chen and J. Jing, Phys. Lett. B **691**, 254-260 (2010).
[73] R. A. Konoplya and A. F. Zinhailo, Phys. Lett. B **810**, 135793 (2020).
[74] P. Boonserm and M. Visser, Annals Phys. **323**, 2779-2798 (2008).
[75] P. Boonserm, [arXiv:0907.0045 [math-ph]].
[76] P. Boonserm and M. Visser, Phys. Rev. D **78**, 101502 (2008).
[77] T. Ngampitipan and P. Boonserm, Int. J. Mod. Phys. D **22**, 1350058 (2013).
[78] P. Boonserm, T. Ngampitipan and P. Wongjun, Eur. Phys. J. C **78**, no.6, 492 (2018).
[79] P. Boonserm, T. Ngampitipan and M. Visser, JHEP **03**, 113 (2014).
[80] P. Boonserm, A. Chatrabhuti, T. Ngampitipan and M. Visser, J. Math. Phys. **55**, 112502 (2014).
[81] T. Ngampitipan and P. Boonserm, J. Phys. Conf. Ser. **435**, 012027 (2013).
[82] P. Boonserm, T. Ngampitipan and P. Wongjun, Eur. Phys. J. C **79**, no.4, 330 (2019).
[83] T. Ngampitipan and P. Boonserm, arXiv:1301.7527 [math-ph].
[84] M. Visser, Phys. Rev. A **59**, 427-438 (1999).
[85] M. Bojowald, Living Rev. Relativity **11**, 4 (2008).
[86] P. Singh, Class. Quant. Grav. **26**, 125005 (2009).
[87] A. Ashtekar and P. Singh, Class. Quant. Grav. **28**, 213001 (2011).
[88] L. Modesto, Class. Quant. Grav. **23**, 5587 (2006).
[89] M. Campiglia, R. Gambini, and J. Pullin, Class. Quant. Grav. **24**, 3649 (2007).
[90] F. Caravelli and L. Modesto, Class. Quant. Grav. **27**, 245022 (2010).
[91] A. Corichi and P. Singh, Class. Quant. Grav. **33**, 055006 (2016).
[92] J. Olmedo, S. Saini, and P. Singh, Class. Quant. Grav. **34**, 225011 (2017).
[93] A. Ashtekar, J. Olmedo, and P. Singh, Phys. Rev. Lett. **121**, 241301 (2018).
[94] F. Zwicky, Astrophys. J, **86**, 217 (1933).
[95] G. Hinshaw *et al.* [WMAP Collaboration], Astrophys. J. Suppl. **208**, 19 (2013).
[96] D. C. Latimer, Phys. Rev. D **88**, 063517 (2013).
[97] Q. M. Fu and X. Zhang , arXiv:2111.07223v1 [gr-qc].
[98] V. Perlick, O. Y. Tsupko and G. S. Bisnovatyi-Kogan, Phys. Rev. D **92**, 104031 (2015).
[99] G. S. Bisnovatyi-Kogan and O. Y. Tsupko, Plasma Phys. Rep. **41**, 562 (2015).
[100] C. R. Keeton and A. O. Petters, Phys. Rev. D **72**, 104006 (2005).
[101] P. Boonserm , C. H. Chen, T. Ngampitipan and P. Wongjun, Phys. Rev. D **104**, 084054 (2021).